REVIEWS OF MODERN PHYSICS VOLUME 15, NUMBER 4 OCTOBER, 1943

Meteors and the Earth's Upper Atmosphere

FRED L. WHIPPLE

Harvard College Observatory, Cambridge, Massachusetts

TABLE OF CONTENTS

1. INTRODUCTION

SINCE 1923 when the pioneer meteor studies by Lindemann and Dobson[1] showed that the density of the earth's upper atmosphere must greatly exceed previously estimated values, it has been realized that the atmospheric temperature may rise with increasing height above the earth's surface in regions well above the stratosphere. Direct measures with radio sonde balloons now provide reliable information as to temperatures up to and above the 30-km level. In higher regions only indirect methods for measuring temperature or density can be utilized.

The anomalous reflection of gun-fire sounds has enabled F. J. W. Whipple[2] and Duckert[3] to predict a rising temperature above the stratosphere to a maximum value somewhere around the 50- to 60-km level. Confirmation of such a temperature maximum is supplied by theoretical considerations proposed by Taylor[4] and extended by Pekeris.[5] To account for two free periods of oscillation in the atmosphere (12^h and $10^h.5$), Pekeris shows that the temperature must again fall at a level immediately above the high temperature region near 60 km. The natural periods of oscillation are suggested by barometric measures and confirmed by the velocities of sound waves observed at great distances from the explosions of the Great Siberian Meteor and the volcanic island of Krakatoa.[6]

In harmony with these conclusions is Humphreys'[7] suggestion that the noctilucent clouds may be composed of ice crystals, which he has shown can be formed over ice at a temperature of 160°K, a temperature much below the value estimated at the 60-km level. Jesse[8] and Størmer[9] have observed that the noctilucent clouds occur in a narrow range of altitude centered at 82 km. This evidence for a low or minimum value of the atmospheric temperature near 82 km is less conclusive, perhaps, than the general evidence for a temperature decrease above the 60-km level, but it encourages confidence in the theoretical result.

Near and above the 100-km level another rise in temperature is required by the energy distribu-

[1] F. A. Lindemann and G. M. B. Dobson, Proc. Roy. Soy. **A102**, 411 (1923).
[2] F. J. W. Whipple, Quart. J. Roy. Met. Soc. **57**, 331 (1931); **58**, 471 (1932); and **60**, 80 (1934).
[3] P. Duckert, Gerlands Beitr. z. Geophys. Suppl. **1**, 280 (1931).
[4] G. I. Taylor, Proc. Roy. Soc. **A126**, 169 and 728 (1929).
[5] C. L. Pekeris, Proc. Roy. Soc. **A158**, 650 (1937).
[6] F. J. W. Whipple, Quart. J. Roy. Met. Soc. **56**, 287 (1930); and **60**, 505 (1934).
[7] W. J. Humphreys, Monthly Weather Review **61**, 228 (1933).
[8] O. Jesse, Astronom. Nach. **140**, 161 (1896).
[9] C. Størmer, Univ. Obs. Oslo, Pub. No. 6 (1933); and Astronom. Norv. **1**, 87 (1935).

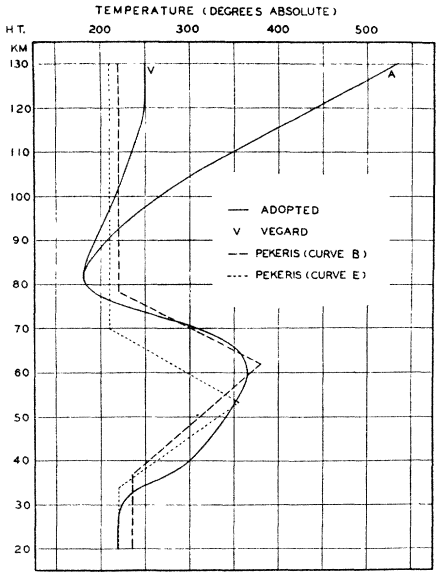

FIG. 1. Atmospheric temperature curves.

tion in the nitrogen bands of the auroral spectrum, observed by Vegard.[10] A temperature of 218°K was obtained by Vegard, but Rosseland and Steensholt[11] have corrected this value to 347°K. It applies approximately at a height of 110 km.

These considerations of the temperature distribution in the upper atmosphere were presented by Martyn and Pulley[12] and led the present writer[13] to adopt the temperature scale of Table I as a working basis for comparison with results obtained from photographic observations of meteors. The consequent values of the air density ρ, in Table I, and the logarithmic gradient $(-1/\rho)(d\rho/dH)$ were obtained on the assumption that the mean molecular weight remains constant at 28.8 throughout the regions considered, and that the pressure is 41 mm Hg and the temperature −58°C (215°K) at a height of 20 km.[14]

TABLE I. Adopted atmospheric conditions.

Height km	T °K	$-\log \rho$	$-\frac{1}{\rho}\frac{d\rho}{dH}$ ×10⁶
20	219	4.06	1.56
25	220	4.40	1.56
30	223	4.74	1.62
35	256	5.12	1.79
40	299	5.45	1.36
45	322	5.73	1.19
50	340	5.97	1.11
55	356	6.21	1.04
60	365	6.42	0.94
65	355	6.62	0.82
70	309	6.78	0.67
75	230	6.93	0.89
80	184	7.20	1.64
85	186	7.62	1.99
90	206	8.04	1.91
95	233	8.44	1.74
100	266	8.79	1.55
105	303	9.11	1.39
110	347	9.46	1.24
115	393	9.71	1.10
120	440	9.94	0.97

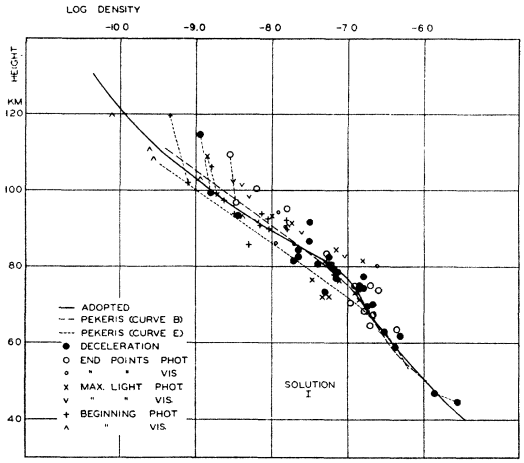

FIG. 2. Uncorrected density data.

The temperature curve of Table I is shown graphically in Fig. 1, along with two trial temperature curves used by Pekeris. The resulting density curves are reproduced in Fig. 2. Throughout this paper c.g.s. units are used for all physical quantities unless other units are explicitly stated.

The aim of the present paper is threefold: first, to present in a convenient form all the published and hitherto unpublished photographic observations of meteors that may contribute to a solution of the problem of upper-atmosphere densities and temperatures; second, to present the adopted theory, both new and old, from a critical viewpoint; and third, to deduce as much as possible about densities and temperatures of the upper atmosphere to a height of about 110 km. An estimate of the probable range of solution

[10] L. Vegard, Geophys. Pub. Oslo, No. 9 (1932); and Nature **138**, 930 (1936).

[11] S. Rosseland and G. Steensholt, Univ. Obs. Oslo, Pub. No. 7 (1933).

[12] D. F. Martyn and O. O. Pulley, Proc. Roy. Soc. **A154**, 455 (1936).

[13] F. L. Whipple, Proc. Am. Phil. Soc. **97**, 499 (1938).

[14] From "Stratosphere flight of explorer, II"; Nat. Geog. Soc. (1936).

TABLE II. Fundamental photographic meteor data.

No.	AI	FA	Yr. and Mo.	Date	Shower	No. breaks	V_∞ km sec.$^{-1}$	$-V_0^\dagger$ km sec.$^{-2}$	p.e.	H_0 km	H_1 km	H_0 km	H_m km	H_L km	H_t km	M Xsec.	M_1	M_0	M_m	Cos Z_R
642	32906	369	'36 Oct.	21.30	Taur.	12	30.65	2.28	±0.16	96.2	90.0	82.4	77.1	75.0	73.8	−1.7	−0.6	−2.3	−2.6	0.815
642						5	29.79	8.4	±0.5			77.4						−2.6		0.815
651	33020	517	'36 Dec.	14.31	Gem.	10	36.56	1.09	±0.53	96.7	93.4	84.3	84.3	75.5	75.1	−1.9	−1.7	−2.8	−2.8	0.978
660	33109	662	'37 Feb.	4.24	Spor.	48	13.26	0.492	±0.039	71.4	69.0	58.9	(54)	(49.4)	(48.1)	(−3.9)	−1.6	−3.0	(−3.2)	0.562
660				4.20			15.47	0.57	±0.05	80.6	77.2	62.9	(56)	(49.4)	(47.7)	(−4.2)	−1.9	−3.3	(−3.5)	0.682
663	33120	690	'37 Feb.	12.24	Spor.	18	79.69	0.34	±0.17	120.2	119.7	114.7	114	110.7	109.4	−3.8	−3.0	−4.0	−4.0	0 123
663				12.22			68.43	0.30	±0.15	102.4	102.1	99.5	99	97.5	96.8	−3.5	−2.7	−3.7	−3.7	0.074
670	33183	792	'37 Mar.	12.36	Spor.	11	23.88	2.07	±0.40	78.5	77.5	74.4	(71.1)	71.3	71.0	−3.1	−2.8	−3.1	−4.8	0.465
689	33416	1171	'37 Aug.	15.26	Per.	6	61.19	10.4	±3.3	106.9	97.4	91.8	91.6	86.3	83.4	−3.0	−3.1	−4.6	−4.6	0.734
694	33530	1362	'37 Oct.	12.35	Spor.	5	69.6	—	—	113.5	106.2	101.3	100.3	96.3	95.2	−1.4	−2.2	—	−3.0	0.681
697	33564	1422	'37 Oct.	31.35	Taur.	15	32.09	3.82	±0.33	99.6	90.9	80.5	76.3	70.8	68.4	−2.0	−0.8	−1.7	−2.8	0.711
697						8	(33.9)	10.0	±1.7			75 0						−2.6		0.711
705	33580	1459	'37 Nov.	5.36	Taur.	15	30.65	0.60	±0.08	105.4	93.9	86.7	83.2	59.5	55.9	−3.7	−0.9	−3.2	−3.8	0.660
705						15	30.20	1.56	±0.15			78.5						−3.4		0.660
705						11	28.47	7.11	±0.40			69.7						−2.8		0.660
705						7	23.64	19.1	±2.2			61.7						−1.5		0.660
710	33589	1480	'37 Nov.	8.21	Taur.	18	30.17	1.75	±0.07	100.4	92.2	80.6	71.9	69.8	67.6	−1.7	−1.2	−1.6	−1.9	0.891
710						9	28.44	7.6	±0.9			74.7						−1.8		0.891
712	33593	1491	'37 Nov.	10.23	Taur.	20	29.20	1.14	±0.04	96.5	94.0	79.4	73.1	65.2	63.5	−4.0	−1.8	−3.7	−4.6	0.897
712						6	28.10	4.5	±0.8			70.2						−4.2		0.897
716	33904†	1494	'37 Nov.	10.38	Taur.	0	29.2‡						81.5						−4.6	0.571
727	33681	1637	'37 Dec.	12.38	Gem.	10	35.21	1.6	±1.4	90.6	89.8	82.7	76.5	75.7	74 3	−0.5	−1.1	−1.5	−1.6	0.891
730	33687	1641	'37 Dec.	13.33	Gem.	16	35.96	2.4	±1.7	95.0	88.3	73.4	(63.2)	59.1	58.1	—	−2.6	−3.5	−4.3	0.968
733	33688	1643	'37 Dec.	13.43	Gem.	16	38.43	0.065	±0.022	107.2	104.9	93.5	(87.6)	83.0	81.7	—	−1.9	−3.5	−4.2	0.768
736	33696	1645	'37 Dec.	14.38	Gem.	15	36.05	1.52	±0.26	94.7	92.7	81.5	81.2	70.6	70.5	−1.0	−0.9	−1.4	−1.7	0.880
778	34257	2310	'38 Oct.	26.34	Taur.	12	33.25	2.62	±0.36	101.2	85.7	77.0	72.0	66.7	64.6	−3.1	−1.3	−3.5	−3.8	0.795
505	4653*	Bright**	'32 Nov.	4.04	Spor.	11	13.6	2.4	±1.1	86.5		47.0	61.2		42.5			−2.4		0.885
505		Faint**				13	13.4	9.4	±0.6			47.0						−1.9		0.885
505		Bright**	'32 Nov.	4.10		11	9.6	1.7	±0.8	71.9		44.8	54.5		41.6			−1.6		0.860
505		Faint**				13	9.5	6.6	±0.4			44.8						−1.2		0.860

† AC plate number. ‡ Assumed. * RH plate number. ** Component of split trail.

is, of course, a fundamental part of the discussion. Certain of the visual observations made by the Arizona expedition for the study of meteors, led by E. Öpik, are included and analyzed for purposes of comparison and for extension of results to greater heights.

The methods of observation and reduction of the photographic meteors have been presented in earlier papers. Two cameras are used, one (FA) located at Cambridge, and the other (AI) located at the Oak Ridge Station of the Harvard Observatory, 37.9 km distant. When a meteor is photographed simultaneously by the two cameras, the spatial position of any point on the trajectory can be determined with great precision by trigonometric methods, the stars forming a precise reference system. The trajectories are essentially straight lines, deviations in direction amounting to 20 minutes of arc are large.

A rotating shutter on one of the cameras (now both) is operated by a synchronous motor and interrupts the exposure at intervals of $0^s.05$. Hence the meteor, usually observable for less than a second, is photographed as a broken line, the separation of successive breaks providing a direct measure of the angular velocity. The positions of these breaks can be reduced to the actual trajectory for the determination of both linear velocity and the deceleration produced by the resistance of the earth's atmosphere. The deceleration is generally small, of the order of 1 km sec.$^{-2}$, and usually can be determined with satisfactory accuracy only for the middle point of the trail. The exponential increase of the atmospheric density with decreasing height, however, is taken into account in the reduction for the deceleration at the middle point. For a few meteors enough breaks are measurable to provide a satisfactory determination of the deceleration at two or more points on a single trail.

The luminosity of the meteor can be measured roughly by comparison of the photographic trail with star images. Essentially the method consists of determining the stellar magnitudes of stars whose images, if mentally beaded in a line on the emulsion, would appear to produce the optical effect of the observed meteor trail. The known linear velocity of the meteoric image on the plate provides a measure of the exposure

time for a distance corresponding to the diameter of the corresponding star image. The stellar exposures are about one or two hours, so that the ratio of exposure times sometimes exceeds a factor of 10^7. This exposure factor is used to determine the stellar magnitude of the meteor at given points along the trail. A correction term is included to allow for the difference in the reciprocity failure of the emulsion at the two levels of intensity. Because the logarithms of the two exposure levels are placed nearly symmetrically with respect to the logarithm of the optimum intensity of the emulsion, the correction term is usually small. The meteoric magnitudes are further reduced to a standard distance of 100 km.

Four points on a single trail are used separately in the determination of the density of the atmosphere, a point near the beginning of the trail, the end point, the point of maximum light, and the middle point. The point near the beginning of the trail is chosen at the first measurable break, where the brightness of the trail may be assumed to correspond to the faintest detectable stars. The trail can be followed by the eye to fainter luminosities, but short breaks are uncertain in position.

The observed data are: heights of the four points, magnitudes or luminosities for all except the end point, the integrated luminosity, the velocity (which generally does not change greatly over the measurable trail), the deceleration at the middle point, and the inclination of the trail to the direction of the zenith. These data are presented and discussed in the following section.

2. THE OBSERVATIONAL DATA FROM METEORS

Table II contains the fundamental observational material for the photographic meteors. The number of the meteor is taken from the Harvard Observatory card catalog for the trail on the AI plate. The plate numbers of the plates taken with the AI and FA cameras are given for further identification. The meteors in recognized showers are designated by Taur. for Taurid, Gem. for Geminid, and Per. for Perseid. Other meteors are designated by Spor. for Sporadic. The number of breaks represents the actual number used in the determination of the velocity V_0 and the deceleration $-V_0'$ in the same column of the table. Where more than one deceleration is measured for a single meteor, the measured breaks usually overlap to a certain extent; hence the measures of deceleration are not completely independent. The probable errors given for the decelerations are determined from the internal agreement of the measured breaks along the trail. The ratio of the probable error to V_0' is rigorously determined, but the absolute values of both V_0 and V_0' depend upon the precise instant of apparition because the cameras continuously follow the diurnal rotation of the stars. For a few meteors (Nos. 660, 663, and 505) the instant of apparition could not be determined from the observational data, so that two solutions, covering most of the possible range of solution, are given.

The heights H are measured in kilometers from sea level. The subscripts signify the following: b, the apparent beginning of the trail on the AI plate (usually earlier than on the FA trail); l, the first measurable break; o, the middle point of that portion of the trail used in the determination of V_0 and V_0' given in the same column; L, the last measurable break; and e, the end point of the AI trail. Values of the heights given in parentheses are uncertain, either because the trail ran off the edge of the plate or because the point was unmeasurable.

The magnitudes M are on a visual system, a constant correction of $+1.8$ mag. having been added to the photographic magnitudes determined by the method described above. This correction is empirical, having been determined by Millman and Hoffleit[15] from meteors observed both visually and photographically and having been checked roughly by the present writer. The magnitude system is subject possibly to a large systematic error (± 1 mag.?). Nevertheless, the system is uniform; the random errors are of the order of 0.4 mag. The magnitudes are corrected to a standard distance of 100 km. If, with Öpik,[16] we define I as the visual intensity measured in ergs sec.$^{-1}$ over the spectral interval from $\lambda 4500$

[15] P. M. Millman and D. Hoffleit, Harvard Ann. **105**, 601 (1937).

[16] E. Öpik, Pub. Obs. Astronom. Tartu **29**, No. 5 (1937).

to λ5700, then

$$\log I = 9.84 - 0.4M. \quad (1)$$

A solar energy distribution curve is assumed.

The quantity $M\times$sec. represents the mean magnitude of the entire meteor had it persisted for one second. The light curve of each meteor was transformed to an intensity scale and integrated in the derivation of $M\times$sec. If $M\times$sec. is substituted for M in Eq. (1), the equation gives the total energy E_∞ of the meteor in ergs over the wave-length interval from λ4500 to λ5700.

In the lower line of Table II Z_R is the zenith distance of the radiant of the meteor. If ds is taken as a differential in distance along the meteor's trajectory at a height H, then

$$dH = -\cos Z_R ds. \quad (2)$$

Certain of the meteors in Table II require special comment. Of the two solutions for No. 660 there is little choice from the astronomical point of view. Fortunately the two solutions give similar results in the determination of atmospheric densities. For meteor 663 the results for the two solutions are widely divergent. The first solution gives an elliptic orbit about the sun while the second is hyperbolic. The parabolic solution lies at about 20 percent of the time interval from the first to the second solution. Meteor 505 is a special case discussed by the author in "Photographic meteor studies, II."[17] The meteor was photographed on a single plate of the RH camera (3-inch aperture F:7). The trail was sinuous because of camera vibrations, the period of which could be determined. The velocity of the meteor could be approximately determined by a method first used by Millman and Hoffleit.[15] Near the end, the trail split in two so that decelerations could be measured for both components. Unfortunately the instant of apparition is unknown; two solutions are therefore given. Meteor 505 is represented in Table II only because it provides values of the deceleration at the lowest heights so far measured.

Meteor 705 also split into two components, the deceleration of only the brighter component being measurable. Because of the split, the calculated densities at the beginning, at maximum light, and at the end are considered unreliable.

TABLE III. Fundamental visual meteor data.

Class	Leo.	Per.	*a*	*b*	*c*	*d*
α_1	8°	40°	0°–45°	45°–65°	65°–90°	>90°
α_1 assumed	8°	40°	25°	55°	80°	105°
V km sec.$^{-1}$	72	61	65	49	32	20
H_b km	119.8	110.8	108.4	103.1	93.1	90.9
H_c km	101.4	98.3	102.4	92.0	89.1	82.8
H_e km	94.3	90.8	86.2	85.9	80.8	80.2
M_z	+0.4	+1.4	+2.2	+2.7	+2.4	+1.9
ΔM_z	0.0	0.0	0.0	+0.2	+0.3	+0.5
M_m	+0.4	+1.4	+2.2	+2.9	+2.7	+2.4
$M\times$sec.	+2.3	+3.2	+3.8	+4.4	+4.0	+3.4
Number	93	114	48	56	86	36

For meteor 670, the brightest point of the trail is a flare (burst or spindle) just at the end. Because the light curve is so abnormal, the density derived from the position of maximum light will be given zero weight. The heights of both the point of maximum light and the end point of meteor 660 are uncertain because the meteor runs off the edges of the plate for both cameras.

Meteor 716 was photographed with the AI camera (1.5-inch aperture, F:8.3) at Oak Ridge and with the FA camera in Cambridge. Only the trajectory is therefore measurable because neither camera was equipped with a rotating shutter at the time. The beginning and end points were off the edges of the plates. The radiant agreed well with that of another Taurid, meteor 712, on the same night so that the velocity could be safely assumed.

With the above limitations, the heights and velocities given in Table II can generally be relied upon as sufficiently accurate for the purpose of atmospheric density determinations. The accuracy of the decelerations can be gauged by the probable errors given. The magnitudes are not susceptible to accurate determination, but do present a uniform system and, fortunately, enter the formulae with little weight. The vagaries of individual meteors remain as the greatest source of error.

The fundamental data for visual meteors are given in Table III. They are taken from Table XXXI of "Results of the Arizona expedition for the study of meteors, VI. Analysis of meteor heights" by Öpik.[18] The statistical data of Table III were derived from 433 shower meteors

[17] F. L. Whipple, Proc. Am. Phil. Soc. **82**, 275 (1940).

[18] E. Öpik, Harvard Ann. **105**, 549 (1936).

observed visually from at least two stations. The two strongest showers, the Leonids and Perseids, are listed separately, the other four classes, a to d, were segregated by Öpik according to the angle α_1 between the apex of the earth's motion at the time of observation and the direction of the radiant. The assumed values of α_1 in Table III were not given by Öpik but were deduced approximately from other more extensive tables in the same publication.

If all shower meteors possessed the same heliocentric velocity, the angle α_1 would be a direct measure of their geocentric velocities V. For the Leonids and Perseids the velocity is known, but for the other four classes the values of V in Table III were deduced on the assumption that the mean heliocentric velocity is 40 km sec.$^{-1}$, probably an upper limit.

The heights given by Öpik were derived from mean reciprocal heights in the manner that he has described. They apply to the beginning points b, the central points c, and the end points e. In Table III Öpik's values of the heights have been corrected to sea level by his suggested correction of +1.9 km. In addition the Leonid heights have been corrected by +0.7 km and the Perseid heights by −1.8 km to allow for the seasonal effect of total amplitude 3.7 km derived by Öpik. All the heights should, therefore, apply closely to mean atmospheric conditions throughout the year in the region of Flagstaff, Arizona.

The quantities M_z are Öpik's determination of the mean zenithal visual magnitudes for the meteors observed. The correction terms ΔM_z were derived on the basis of the uncorrected heights, to reduce the zenithal magnitudes to a distance of 100 km, in conformity with the magnitudes given for the photographic meteors. The corrected magnitude M_m will be taken to apply at maximum light. In the derivation of $M\times$sec., the mean time of endurance of each group of meteors is taken to be $(H_b-H_e)/(0.7V)$, in seconds, on the assumption that $\cos Z_R=0.7$. It is further assumed that the meteors were of magnitude +4.2 when first observed and that they were followed by the eye until they reached magnitude +5.5. Thus $M\times$sec. is derived by the numerical integration of an assumed intensity curve in which the maximum light is of magnitude M_m.

The number of individual meteors upon which the results for each class depend is given in the bottom line of Table III.

3. THEORETICAL CONSIDERATIONS

The contributions by Öpik[19] and Hoppe[20] have been the principal direct sources of material for the theory adopted in the determination of atmospheric densities from meteoric data. The basic assumptions and equations can advantageously be discussed individually in order to outline the ground framework of the theory. The discussion will be divided in subsections as follows: (a) the resistance equation; (b) the equation for the loss of mass; (c) the luminosity equations; (d) density from the deceleration; (e) density at maximum light; (f) density near the beginning point; (g) density at the end point; (h) adopted values of the constants.

(a) The Resistance Equation

Perhaps the most reliable equation is that for the atmospheric resistance to a meteoroid. The greatest uncertainty probably rests in the unknown but certainly irregular shape of the meteoric body. If, at any time, the total mass is m, let us define a quantity A such that $Am^{\frac{2}{3}}$ is the area of the effective cross section exposed to atmospheric resistance. For a sphere of specific density ρ', $A^3=9\pi/16\rho'^2$. For a cone of revolution with semi-angle θ, $A^3=9\pi\tan^2\theta/\rho'^2$, if the vertex of the cone is pointed in the direction of motion. If the cone is symmetrical about the base so that a second vertex points opposite to the direction of motion, $A^3=9\pi\tan^2\theta/4\rho'^2$.

Given a velocity V through an atmosphere of density ρ, the meteoroid will encounter an air mass dm_a in time dt, where

$$dm_a=Am^{\frac{2}{3}}\rho V dt. \qquad (3)$$

Because the velocity of a meteor always exceeds the velocity of sound by a large factor, the shock wave will be exceedingly thin and will lie on the forward surface of the meteoroid. Hence we may reasonably assume that only the

[19] E. Öpik, Veröff. Dorpat **25**, 1 and 32 (1922); Harvard Reprint No. 100 (1933).
[20] J. Hoppe, Astronom. Nach. **262**, 169 (1937).

column of air actually lying within the column cut out by the body itself will produce a resistance and that a unit mass of air in this column receives a component of momentum γV along the direction of motion (where γ is a dimensionless constant). The meteor thus experiences an acceleration V', given by

$$V' = dV/dt = -\gamma A m^{-1/3} \rho V^2. \quad (4)$$

There is universal agreement as to the form of this expression for velocities much above the velocity of sound. The constant γ is independent of the velocity and depends only upon the shape of the moving body. In his "energy trap" process Öpik suggests that the air particles penetrate the material (solid or liquid) of the meteoroid's surface, are momentarily carried along with the meteoroid, and then are brushed away with a relatively small velocity. In this case $\gamma = 1.0$.

For projectiles at smaller velocities, still well above the velocity of sound, the observed and theoretical values of γ are in good agreement and are considerably smaller. Epstein's[21] equations lead to $\gamma = \frac{1}{3}$ for a spherical projectile. Taylor and Macoll,[22] and Macoll[23] have investigated by theoretical and experimental methods the air pressure on a cone moving at high speeds. Their results are given in terms of $(p_s - p_1)/\rho V^2$, where p_s is the air pressure at the forward surface of the cone and p_1 is the normal air pressure. Since p_1 is negligible compared to p_s in our problem, and since $p_s \times$surface area, for a right-circular cone with the axis and vertex pointed in the direction of motion, gives a total resistance force of $p_s \times A m^{\frac{2}{3}}$, we find that $(p_s - p_1)/\rho V^2$ is identical with γ.

The last column of Table IV contains the values of γ taken from the results obtained by Taylor and Macoll. The argument θ is the semi-angle at the vertex of the cone. I have extrapolated their values slightly for the asymptotic values that would clearly result at velocities much greater than the maximum velocities they studied, some 5 to 8 times the velocity of sound. The second column of Table IV contains the value of A for a stone of density $\rho' = 3.4$. The third column is similarly obtained for a double symmetrical cone with the second vertex pointing away from the direction of motion. For a sphere of density 3.4, $A = 0.53$.

TABLE IV. Resistance factors for a moving cone.

θ	A (Single cone)	A (Double cone)	γ
10°	0.42	0.27	0.03
20°	0.69	0.43	0.12
30°	0.93	0.59	0.26
40°	1.20	0.76	0.43
50°	1.52	0.95	0.62
55°	1.71	1.08	0.73

It is obvious from Table IV that a moderate uncertainty must exist in the value to be adopted for γ. Öpik[24] has suggested that meteors have been set in rapid rotation by collisions in space. If so, we might expect them generally to rotate about a minor axis; hence a fairly large value of γ would be applicable. There is no direct evidence, however, for such rotation.

Because the values of γ and A are correlated, the difficulty of obtaining a reliable mean value of the product is increased. A long, thin meteoroid, if such exists, might orient itself with the major axis along the direction of flight with a consequent small value of γA. On the other hand, a flat thin meteoroid might generally present the flat surface (e.g., falling ice crystals) and give a very high value for γA.

Öpik's arguments for the energy trap hypothesis, however, must not be discounted. Voorhis and Compton[25] find that the accommodation coefficients of positive ions of argon, neon, and helium are surprisingly high. At velocities of from 10 to 80 km sec.$^{-1}$ the positive ions appear to penetrate a solid metallic surface to much greater depths than at low velocities corresponding to normal temperatures. Hence their energy and, of course, their momentum are largely transferred to the surface which they strike. By a long and involved argument, Öpik shows that no air cap can form to protect a small meteoroid from the penetration process. Thus for the photographic and visual meteors with which we are concerned the value of γ must be high, not far

[21] P. S. Epstein, Proc. Nat. Acad. Sci. **17**, 532 (1931).
[22] G. I. Taylor and J. W. Macoll, Proc. Roy. Soc. **A139**, 278 and 298 (1933).
[23] J. W. Macoll, Proc. Roy. Soc. **A159**, 459 (1937).
[24] E. Öpik, Pub. Obs. Astronom. Tartu **28**, No. 6, 13 (1936).
[25] C. C. Van Voorhis and K. T. Compton, Phys. Rev. **37**, 1596 (1931).

from unity. For much more massive fireballs, which are not destroyed in the upper atmosphere, smaller values of γ probably are applicable.

The value of A depends not only upon the shape and orientation of the meteoroid but also upon its specific density. Watson,[26] in a recent summary of the composition of meteorites observed to fall, finds that stony meteorites are more prevalent than iron meteorites by a factor of more than ten. The older notion that irons are more prevalent is based on the recorded *finds* of meteors. An iron is much more readily recognized than a stone after weathering has set in. We may therefore safely leave the iron meteoroids out of consideration and consider only stony material, which, incidentally, contains some 25 percent iron by mass.

In previous papers the values $\gamma=1.0$ and $A=0.5$ were adopted. From the above discussion it is apparent that γ might well be decreased to perhaps 0.9 or 0.8, but that A should probably be increased, perhaps to about unity. The old product, $\gamma A=0.5$, should probably be increased (perhaps to about 0.9). In the calculations to follow, the old values are retained, but it will be of interest to note the effect of an increase in γA.

Returning to the fundamental Eq. (4), it is important to note that the exponent of V is probably correct, that no error dependent upon the velocity should be expected. Random errors of considerable magnitude, however, may arise in the coefficient A. Also the value of A may possibly decrease as the meteoroid passes through the atmosphere. Vaporization generally should tend to remove the rough edges and reduce the ratio of cross section to mass. Otherwise the resistance equation appears to be entirely reliable.

(b) The Equation for the Loss of Mass

The energy dW, available for heating, melting, and vaporizing the material of the meteoroid, in a time dt, will be proportional to the air mass encountered times one-half the square of the velocity. The factor of proportionality $\bar{\lambda}$ will depend upon the final velocities of the air molecules (now atoms) and the efficiency of the process in heating the surface of the meteoroid. We may write

$$dW=\tfrac{1}{2}\bar{\lambda}Am^{\frac{2}{3}}\rho V^3dt. \tag{6}$$

In the energy trap process practically all of the energy of collision with air molecules can be utilized in heating the meteoroid. Hence $\bar{\lambda}$ is large, of the order of unity. With $\gamma=1$ the total energy lost to the meteor per second is $Am^{\frac{2}{3}}\rho V^3$, of which one-half is utilized in transmitting the velocity of the meteor to the air mass encountered. With perfect efficiency the other half would be absorbed by the material of the meteoroid as dW, of Eq. (6). Hence $\bar{\lambda}/\gamma$ measures the effeciency of the heating (or absorption of energy) process.

The "accommodation coefficients" determined by Van Voorhis and Compton are essentially equivalent to $\bar{\lambda}$ and are equal to 0.75 for positive argon ions and 0.65 for neon, at velocities comparable to the slower meteors. The coefficients appear to increase both with molecular weight and velocity. Öpik adopts a value of $\bar{\lambda}=0.60$ (χ in his notation), as a conservative estimate. (Some energy, of course, is lost in direct material radiation.) Sparrow[27] adopts a smaller value of 0.37.

The energy dW will be used in heating the material of the meteoroid from a low temperature until either it melts and is brushed away in droplets or it is vaporized and lost as a gas. At the moment we need not dwell on the problem of deciding between the two processes. If ζ represents the energy in ergs required either in melting or vaporizing a gram of the material the rate of loss of mass becomes [from Eq. (6)]

$$dm/dt=-(\bar{\lambda}/2\zeta)Am^{\frac{2}{3}}V^3, \tag{7}$$

the second fundamental equation.

Averaged values of the relevant physical constants for stone meteorites have been obtained by Öpik and are presented in Table V. From these constants values of ζ are derived, first to melt the material from 280°K, and second to vaporize the material from 280°K. For iron meteorites the values of ζ are essentially the same.

It is likely that material is being lost both by spraying of fine droplets and by evaporization. Öpik discusses these problems in some detail, but it is hardly necessary here to mention more than a few points. The conductivity of iron is some

[26] F. Watson, *Between the Planets* (The Blakiston Company, Philadelphia, 1941), pp. 140 and 177.

[27] C. M. Sparrow, Astrophys. J. **63**, 90 (1926).

twenty times greater than that for stone; hence the problem of melting and spraying is more serious for iron meteorites than for stone. A visual meteor of stone with a radius of the order of 1 mm is probably entirely melted before it becomes luminous. A larger photographic meteor with a diameter of the order of 1 cm is probably molten only in a surface layer. If such a meteor is rapidly rotating the rate of loss of material will be considerably more rapid than if it is slowly rotating because the centrifugal force will throw off droplets.

It is fortunate that the various methods of determining atmospheric densities from photographic meteors provide a determination of the quantity $\zeta\gamma/\bar{\lambda}$. We can therefore use this derived value without entering into a more thorough discussion of the actual process of the loss of mass. In earlier papers the values $\zeta=6\times10^{10}$ and $\bar{\lambda}=0.5$ were adopted. This value of ζ corresponds to the heat of vaporization alone. Then, $\zeta\gamma/\bar{\lambda}=1.2\times10^{11}$, a value in good agreement with the observational material. If we should choose to adopt $\bar{\lambda}=0.6$ and $\gamma=0.9$, then $\zeta=8.0\times10^{10}$, a fair confirmation of the assumption that the material of the meteoroid is completely volatilized before it leaves the surface.

These suggested changes in the values of the constants leave the value of $\bar{\lambda}/\zeta$ in Eq. (7) practically unaltered. The previously adopted value, therefore, is used in the calculations of density in Section 4, below. The power of V in Eq. (7) must be essentially correct. The quantities $\bar{\lambda}$ and A both will probably decrease somewhat for a given meteor along its trajectory. On the other hand, the effective value of ζ may also decrease as a greater atmospheric pressure tends to brush off droplets before the material is vaporized. Hence Eq. (7) should be statistically reliable and subject to a rather small change in the course of a given meteor.

Two auxiliary equations of importance can now be derived. The ratio of Eq. (7) to Eq. (4) gives a differential equation between m and V in which the atmospheric density and the time have been eliminated. If the subscript ∞ refers to the quantities just outside the earth's atmosphere, we derive the relation:

$$\ln(m/m_\infty)=(\bar{\lambda}/4\gamma\zeta)(V^2-V_\infty^2), \tag{8}$$

TABLE V. Physical data for stone meteorites.

Specific heat of solid	1.1×10^7 ergs g^{-1} deg.$^{-1}$
Specific heat of liquid	1.3×10^7 ergs g^{-1} deg.$^{-1}$
Heat of fusion	0.3×10^{10} ergs g^{-1}
Heat of vaporization	5.6×10^{10} ergs g^{-1}
Melting point	1800°K
Boiling point	3000°K
ζ to melt from 280°K	2.0×10^{10} ergs g^{-1}
ζ to vaporize from 280°K	9.1×10^{10} ergs g^{-1}

connecting the mass and velocity independently of time.

If s is the linear distance measured along the trajectory, Eq. (7) may be rewritten

$$dm/m^{\frac{1}{3}}=-(\bar{\lambda}/2\zeta)A\rho V^2ds. \tag{9}$$

By integration we obtain

$$m^{\frac{1}{3}}=m_\infty^{\frac{1}{3}}-\frac{\bar{\lambda}A}{6\zeta}\int_{-\infty}^{s}V^2\rho ds. \tag{10}$$

Since the deceleration of the meteor is relatively small, V may be assumed constant with little error and the V^2 term removed from the integral of Eq. (10). A relation is thus obtained between the mass of the meteor at any point along its trajectory and the mass of the atmosphere through which it has passed.

(c) The Luminosity Equations

The blackbody radiation at the surface of the meteoroid can be shown to represent only a small fraction of the luminosity for the relatively small masses in the photographic or visual meteors under consideration. This fact has been recognized by practically all theoretical workers in the field. The principal source of the visual or photographic radiation occurs in a coma of vaporized meteoric material around and behind the meteoroid itself. Practically all the original energy is expended as the cloud of meteoric atoms collides with the molecules of the atmosphere *after* the meteoric material has left the main body. For a meteor of velocity only 10 km sec.$^{-1}$, the original kinetic energy is 5×10^{11} ergs g^{-1}, more than five times the energy needed for vaporization.

We may simply assume, therefore, that the luminosity I is proportional to the energy of the mass lost per second times τ, a luminous efficiency factor. The luminosity is then

$$I=-\tfrac{1}{2}(dm/dt)V^2\tau. \tag{11}$$

Substituting dm/dt from Eq. (7), we have

$$I=(\tau\bar{\lambda}A/4\zeta)m^{\frac{2}{3}}\rho V^5. \quad (12)$$

An evaluation of τ has been taken from the calculations by Öpik. His analysis is long and only the briefest summary will be attempted. He has calculated the radiation energy emitted in the wave-length range λ4500 to λ5700 by the iron atoms in a cloud through which a stream of nitrogen atoms is moving at specific high velocities. He has assumed (a) ionization potentials and the law of atomic interaction as for nitrogen and iron; (b) excitation, or radiation potentials evenly distributed within the given interval of ionization energy, and radiation of the type of ultimate lines; (c) a short lifetime for an excited state as compared with the time between two collisions.

For the brighter meteors, in the photographic range, his calculations are well represented by the formula

$$\tau=\tau_0 V, \quad (13)$$

where $\log\tau_0=-9.07+\log V$ (cm^{-1} sec.). The intensity I must represent only the energy in the interval λ4500 to λ5700.

For the fainter visual meteors he assumes that the physical process is more that of single Fe atoms moving through a cloud of N atoms, which he shows produces only $\frac{1}{4}$ the Fe radiation per unit energy of the moving atoms. His tabular values include a smoothing for the transition region from one assumption to another. The luminous efficiency for the visual meteors is roughly approximated by a constant, $\log\tau=-3.10$. The above evaluations of τ have been adopted in the present calculations.

(d) Density from the Deceleration

We wish to derive an expression for the density ρ in terms of the velocity, deceleration, and the intensity; the intensity can be obtained from the observed magnitudes by Eq. (1). The mass is expressed by Eq. (4), giving

$$m^{\frac{1}{3}}=-\gamma A\rho V^2/V'. \quad (14)$$

The expression for τ in Eq. (13) is substituted in Eq. (12) and the mass eliminated by Eq. (14).

The expression for ρ_0 at the zero point where the deceleration is known then becomes

$$\rho_0=K_0 V_0^{-10/3}(-V_0)^{2/3}I_0^{1/3}, \quad (15)$$

where

$$K_0^3=4\zeta/(\bar{\lambda}\gamma^2\tau_0 A^3). \quad (16)$$

Of the greatest importance is the fact that in Eq. (15), as in all of the solutions for density, the intensity I and the luminous efficiency factor τ_0 enter only to the one-third power. Also the power of V in the expression for τ enters only to the one-third power. As a consequence, the rather large uncertainties in the magnitude system and in the equation of luminous efficiency affect the calculated values of density only slightly. An error of one magnitude produces an error of only 0.13 in $\log\rho$. Even an error of a factor of 10 in the luminous-efficiency equation would change $\log\rho$ by only 0.33. Since errors of this type should be largely systematic, the effect is simply to raise or lower the entire $H-\log\rho$ curve, with no change in the slope, i.e., with no change in the derived atmospheric temperature in the region covered by the calculations. An error in the exponent of V in the equation of luminous efficiency, however, will produce a small change in the derived atmospheric temperatures.

(e) The Density at Maximum Light

The intensity equation (12), when differentiated logarithmically for the maximum intensity, gives

$$\frac{2}{3m}\frac{dm}{dt}+\frac{1}{\rho}\frac{d\rho}{dt}+\frac{6}{V}\frac{dV}{dt}=0, \quad (17)$$

if $\tau=\tau_0 V$ for photographic meteors. The first term in Eq. (17) can be derived by solving for m and dm/dt separately from Eqs. (11) and (12) as follows:

$$\frac{dm}{dt}=-\frac{2I}{\tau V^2}=-\frac{\lambda A}{2\zeta}m^{\frac{2}{3}}\rho V^3, \quad (18)$$

whence

$$m^{\frac{2}{3}}=4I\zeta/(\tau\bar{\lambda}A\rho V^5). \quad (19)$$

The second term in Eq. (17) must be evaluated from an assumed curve of density against height H in the atmosphere. Since $dH=-\cos Z_R ds$ and $V=ds/dt$

$$\frac{1}{\rho}\frac{d\rho}{dt}=-V\frac{1}{\rho}\frac{d\rho}{dH}\cos Z_R=Vb\cos Z_R, \quad (20)$$

if $-b$ is defined as the logarithmic density gradient $d\rho/(\rho dH)$.

In an isothermal atmosphere b is simply $-g\mu/(kT)$, where g is the acceleration of gravity, μ is the mean molecular weight, k is Boltzmann's constant, and T is the absolute temperature. In a heterothermal atmosphere, b also depends upon the temperature and its gradient with height. Table I gives values of b for the adopted atmosphere.

The third term in Eq. (17) is evaluated from Eq. (4), an expression for $m^{-\frac{1}{3}}$ being provided by Eq. (19). Finally the density at maximum light becomes

$$\rho_m = K_m N V_m^{-10/3} I_m^{1/3} (b \cos Z_R)^{2/3} \qquad (21)$$

for photographic meteors, and

$$\rho_m = K_m' N' V_m^{-3} I_m^{\frac{1}{3}} (b \cos Z_R)^{\frac{1}{3}} \qquad (21a)$$

for visual meteors.

The quantities N and N' are near unity numerically but are not negligible.

$$N^{-\frac{1}{3}} = 1 + 18\gamma\zeta/(\bar{\lambda} V_m^2), \qquad (22)$$

and

$$N'^{-\frac{1}{3}} = 1 + 15\gamma\zeta/(\bar{\lambda} V_m^2). \qquad (22a)$$

The constant terms are:

$$K_m = 6^{\frac{1}{3}}\zeta/(\bar{\lambda} A \tau_0^{\frac{1}{3}}), \qquad (23)$$

and

$$K_m' = 6^{\frac{1}{3}}\zeta/(\bar{\lambda} A \tau^{\frac{1}{3}}). \qquad (23a)$$

It should be noticed that Eq. (21), when applied to an actual meteor, depends for its accuracy upon the precision with which the luminosity curve of the meteor follows the theoretical luminosity curve specified by the fundamental equations. The agreement between theory and observation appears to be good statistically, but the random error is great from meteor to meteor. Hence densities calculated from the data at maximum light may be expected to show larger deviations from the mean than densities calculated from the decelerations.

(f) Density near the Initial Point

The equation for atmospheric density to be derived in this section is intended to apply at any early point of the trail where the luminosity can be measured, but before the meteor has lost an appreciable fraction of its mass or velocity. If we disregard the deceleration of the main body of the meteoroid during its flight, the total luminous energy E_∞ defined above, should be a direct measure of its initial mass m_∞. By the principle used in deriving Eq. (11) we have

$$m_\infty = 2E_\infty/(\tau V^2), \qquad (24)$$

probably an underestimate of m_∞, but not a gross underestimate.

A substitution of this value for m_∞ in the luminosity equation (12) gives immediately an expression for the density near an initial point,

$$\rho_1 = K_1 I_1 E_\infty^{-\frac{1}{3}} V_\infty^{-4} \qquad (25)$$

for photographic meteors, and

$$\rho_1 = K_1' I_1 E_\infty^{-\frac{1}{3}} V_\infty^{-4\frac{1}{3}} \qquad (25a)$$

for visual meteors.

The constants are:

$$K_1 = 2^{4/3}\zeta/(\lambda A \tau_0^{\frac{1}{3}}), \qquad (26)$$

and

$$K_1' = 2^{4/3}\zeta/(\bar{\lambda} A \tau^{1/3}). \qquad (26a)$$

Since the value of $m^{-\frac{1}{3}}$ used in the derivation of Eq. (25) is probably too small, the resultant value of ρ_1 will be too large. A partial compensation for this error can be made by using a maximum value of V in the equations, i.e., V_∞, the velocity of the meteor before it encountered the atmosphere. Equation (25) in practice gives about the same random errors in $\log \rho$ from meteor to meteor as does the maximum-light equation. It may possibly be subject to somewhat more serious systematic errors than the maximum-light equation because of lags in heating or melting before the meteor becomes luminous. In the present state of the problem, however, even a rough determination of the density near the beginning of the trails is of great value in extending the calculations to greater heights.

(g) Density at the End Point

A fair approximation for the atmospheric density at the last visible point of a meteor trail can be made by neglecting the change of velocity. The original mass of the meteoroid is obtained from the total luminosity [as in Section 3 (f)]. We then assume that this mass has been completely destroyed by spraying and evaporation as the meteor intercepts a column of atmosphere

above the end point. When the right member of Eq. (10) is set equal to zero, V^2 removed from inside the integral, and m_∞ substituted from Eq. (24), we find for the total mass of atmosphere along the trail above the end point

$$\int_{-\infty}^{s} \rho ds = \frac{2^{4/3} 3 E_\infty^{1/3}}{\bar{\lambda} A \tau^{1/3} V^{8/3}}. \tag{27}$$

The left member of Eq. (27) is simply (cos Z_R ×pressure)/acceleration of gravity at the end point of the trail and becomes

$$\int_{-\infty}^{s} \rho ds = \frac{1}{\cos Z_R} \int_{H}^{\infty} \rho dH = \frac{\rho k T}{g \mu \cos Z_R}. \tag{28}$$

Equating the right members of Eqs. (27) and (28), we evaluate the density at the end point

$$\rho_e = K_e V_0^{-3} E_\infty^{\frac{1}{3}} b' \cos Z_R \tag{29}$$

for photographic meteors, and

$$\rho_e = K_e' V^{-8/3} E_\infty^{1/3} b' \cos Z_R \tag{29a}$$

for visual meteors.

The constants are

$$K_e = 3(2)^{4/3} \zeta / (\bar{\lambda} A \tau_0^{1/3}), \tag{30}$$

$$K_e = 3(2)^{4/3} \zeta / (\bar{\lambda} A \tau^{1/3}), \tag{30a}$$

and

$$b' = g\mu/(kT). \tag{31}$$

For an isothermal atmosphere b' is identical with b.

It is clear from the derivation of ρ_e that Eq. (29) must be applied at a point in the trail before the velocity has greatly decreased but after practically all of the mass of the meteor has disappeared. Since photographic meteors can be observed visually some distance farther than they are photographed, it seems that the end point of the photographic trail probably represents well the conditions postulated in the derivation of Eq. (29). Only a very small percentage of the light is emitted beyond this point, and the velocity is still comparable with the original velocity for average meteors.

The equation for the density at the end point represents rather basic conditions for the average meteor. In practice the individual meteors appear to show less random errors in the density at the end point than at an initial point or at maximum light.

(h) The Adopted Values of the Constants

For convenience, the adopted values of the numerical constants are given in Table VI. The units are in the c.g.s. system throughout, and the temperature is expressed in degrees absolute. Certain recommended changes in these constants have been suggested above. A general comparison of the various methods of determining the atmospheric density and the possible changes in the constants will be discussed in Section 5.

4. RESULTS: DENSITIES AND TEMPERATURES

The equations and constants of Section 3 have been used in conjunction with the observed meteoric data of Tables II and III to provide values of the logarithms of the atmospheric density given in Table VII, columns 4, 7, 10, and 13. The corresponding heights, in km above sea level, at which these density determinations apply are given in the preceding columns, Nos. 3, 6, 9, and 10, respectively. The deviations Δ of the observed values of log ρ from those of the adopted density curve (Table VII minus Table I) are given in columns 5, 8, 11, and 14 (the unit of Δ is 0.01 in log ρ). The densities calculated by means of Eq. (15) are tabulated under the heading Deceleration, those by Eqs. (21) and (21a) under Max. light, those by Eqs. (25) and (25a) under First break and those by Eqs. (29) and (29a) under End point.

Column two of Table VII contains the temperature deviations in degrees Fahrenheit from the average mean temperature in Boston. The U. S. Weather Bureau in Boston kindly provided the mean (max. min.) temperatures for the days preceding and following the nights on which the meteors were observed. Temperatures for comparison with density variations in the upper atmosphere were arbitrarily taken as two-thirds the observed mean temperature for the day preceding plus one-third the observed mean temperature for the day following. The average seasonal range in mean temperature at Boston is from 27°F (288°K, Jan. 21 to Feb. 1) to 72°F (313°K, July 10 to Aug. 6). The average value of the daily means was taken as 50°F (301°K).

The density determinations of Table VII are plotted against the corresponding observed heights in Fig. 2. In a few instances, where the

times of the meteors were uncertain, two extremal values of the densities are plotted and connected by dotted lines. For purposes of comparison the density curves corresponding to the upper atmosphere temperature curves of Fig. 1 (and Table I) are also plotted. It is apparent that the adopted density curve and Pekeris' curve B fit the observations appreciably better than Pekeris' curve E. A straight line in the $H-\log\rho$ diagram, corresponding to a constant temperature in the upper atmosphere, would be less satisfactory. The inadequacy of the constant-temperature solution is even more marked when we note that the straight line must connect with the better-known densities in the 30-km to 40-km region.

Hence the meteoric data support the suggestion of a high temperature zone near or slightly above the 60-km level of the atmosphere.

The determination of the best $H-\log\rho$ curve to satisfy the meteoric data is complicated by several factors and must be accomplished by successive approximation. Systematic differences in $\log\rho$ undoubtedly exist among the various methods used. The mean residuals (mean Δ) in Table VII are not a satisfactory measure of these differences because of systematic differences in height. The first observed break must of necessity correspond to a greater average height than the end point, etc. In addition, the heights are closely correlated with the velocities, and the velocities, by chance, are somewhat correlated with the season or mean temperature. A seasonal effect in $\log\rho$ may therefore affect the systematic differences between the various methods even at the same observed height. Finally, the determinations of $\log\rho$ at maximum light and at the end point depend to some extent upon the slope of the assumed $H-\log\rho$ curve.

TABLE VI. Adopted values of the constants.

λ	0.5	$\log K_0$	7.22
γ	1.0	$\log K_1$	14.80
ζ	6×10^{10}	$\log K_1'$	12.81
A	0.5	$\log K_m$	14.92
μ	28.8	$\log K_m'$	12.93
$\log\tau_0$	−9.07	$\log K_e$	15.28
$\log\tau$	−3.10	$\log K_e'$	13.29

$b=d\rho/(\rho dH)$ (Table I or $b=b'$ if $T=$constant)
$b'=g\mu/(kT)=3.41\times10^{-4}/T$
$I=9.84-0.4M$, $E_\infty=9.84-0.4M\times$sec.
$N^{-\frac{1}{2}}=1+2.16\times10^{12}/V_m^2$
$N'^{-\frac{1}{2}}=1+1.80\times10^{12}/V_m^2$.

The determinations of $\log\rho$ from deceleration measures should be more reliable than the other determinations. The residuals of Table VII confirm this expectation although the end-point residuals are surprisingly consistent. In the second solution for the $H-\log\rho$ curve, a preliminary evaluation of the seasonal effect was made from the deceleration residuals alone. These residuals divided by the appropriate values of the slope (b) of the $H-\log\rho$ curve were correlated with the deviations in the ground temperature as though the upper atmosphere as a whole were raised or lowered by temperature changes below. An increase of 1°K in the mean ground temperature was found to correspond to an upward shift of 0.15 km for the atmospheric levels under consideration.

The material of Table VII was then divided into four groups according to the observed height. Within each group the mean residuals in $\log\rho_m$, $\log\rho_1$, and $\log\rho_e$ were compared with the mean residuals in $\log\rho_0$ and the mean difference in each comparison weighted proportionally to the number of the *less* frequently observed class. These weighted differences were then averaged for the four groups and a correction included for the small mean differences in temperature. The results are

$$\begin{aligned}\langle\log\rho_0-\log\rho_m\rangle_{Av}&=+0.06,\\ \langle\log\rho_0-\log\rho_1\rangle_{Av}&=+0.08,\\ \langle\log\rho_0-\log\rho_e\rangle_{Av}&=-0.09.\end{aligned}\qquad(31)$$

It will be noted that these mean differences are somewhat changed from the values directly obtainable from the mean Δ's given in Table VII.

The mean residual in $\log\rho$ for each height group was then derived on the scale of the deceleration determinations by the application of the mean corrections of Eqs. (31) to the values of $\log\rho$ given in Table VII. In deriving the mean residuals for the height groups a single good-quality determination of $\log\rho_0$ was given twice the weight of other determinations. Small corrections were made to allow for deviations from the average ground temperature.

Table VIII contains, for each of the four groups, the limits in height, the mean height, the mean ($\Delta\log\rho$) correction to the density given in Table I, and the corrected value of $\log\rho$. These

TABLE VII. Solution I. Atmospheric densities.

Meteor number	Temp. °F	Deceleration			Max. light			First break			End point		
		H_0 km	$-\log \rho_0$ obs.	Δ $O-C$	H_m km	$-\log \rho_m$ obs.	Δ $O-C$	H_1 km	$-\log \rho_1$ obs.	Δ $O-C$	H_e km	$-\log \rho_e$ obs.	Δ $O-C$
Photographic Meteors													
642	+14	82.4	7.24	+16	77.1	7.15	−11	90.0	8.08	−04	73.8	6.59	+34
642		77.4	6.78	+28	——	——	——	——	——	——	——	——	——
651	−18	84.3	7.65	−09	84.3	7.16	+40	93.4	8.00	+31	75 1	6.70	+26
660	−28	58.9	6.38	00	——	——	——	——	——	——	——	——	——
660		62.9	6.52	+02	——	——	——	——	——	——	——	——	——
663	−21	114.7	8.95	(+84)	114.0	8.85	(+89)	119.7	9.34	( )	109.4	8.56	( )
663		99.5	8.81	(−05)	99.0	8.72	(00)	102.1	9.11	(−18)	96.8	8.47	(+15)
670	−21	74.4	6.80	+11	(71.1)	6.84	(−03)	77.5	7.14	−08	71.0	6.42	+40
689	+22	91.8	7.50	+68	91.6	7.73	+44	97.4	8.63	−02	83.4	7.28	+45
694	−2	101.3	——	——	100.3	8.21	+60	106.2	8.79	+40	95.2	7.80	+73
697	+4	80.5	7.24	00	76.3	7.26	−26	90.9	8.16	−05	68.4	6.78	+02
697		75.0	6.84	+09	——	——	——	——	——	——	——	——	——
705	−7	86.7	7.51	+25	83.2	(6.91)	(+56)	93.9	8.49	(−14)	(55.9)	6.62	(−22)
705		78.5	7.18	−06	——	——	——	——	——	——	——	——	——
705		69.7	6.74	+03	——	——	——	——	——	——	——	——	——
705		61.7	6.36	+13	——	——	——	——	——	——	——	——	——
710	−1	80.6	7.39	−14	71.9	7.33	−49	92.2	7.81	+41	67.6	6.66	+11
710		74.7	6.85	+07	——	——	——	——	——	——	——	——	——
712	+3	79.4	7.19	−02	73.1	6.90	−03	94.0	8.13	+23	63.5	6.36	+27
712		70.2	6.67	+12	——	——	——	——	——	——	——	——	——
716	+3	——	——	——	81.5	6.80	+52	——	——	——	——	——	——
727	−25	82.7	7.65	−22	76.5	7.47	−46	89.8	7.80	+22	74.3	6.88	+08
730	−27	73.4	7.30	−42	——	——	——	——	——	——	——	——	——
733	−27	93.5	8.44	−12	——	——	——	——	——	——	——	——	——
736	−29	81.5	7.72	−40	81.2	7.35	−05	92.7	8.05	+21	70.5	6.97	−17
778	+1	77.0	7.16	−12	72.0	7.24	−40	85.7	8.31	−63	64.6	6.70	−03
505*	−11	47.0	5.86	(−04)	——	——	——	——	——	——	——	——	——
505*		44.8	5.56	(+16)	——	——	——	——	——	——	——	——	——
Mean Δ	——	——	——	——	+02	——	——	+01	——	——	+09	——	——	+22
P.E. Δ	——	——	——	——	±16	——	——	±28	——	——	±20	——	——	±17
Visual Meteors													
Leo.	0	——	——	——	101.4	8.40	+48	119.8	10.12	−19	94.3	7.92	+46
Per.	0	——	——	——	98.3	8.30	+37	110.8	9.62	−10	90.8	7.82	+38
a	0	——	——	——	102.4	8.52	+42	108.4	9.56	−21	86.2	7.95	−23
b	0	——	——	——	92.0	8.19	+01	103.1	8.95	+04	85.9	7.71	−02
c	0	——	——	——	89.1	7.62	+35	93.1	8.38	−09	80.8	7.22	+04
d	0	——	——	——	82.8	7.04	+39	90.9	7.79	+32	80.2	6.62	+60
Mean Δ	——	——	——	——	——	——	——	+34	——	——	−04	——	——	+21

* Mean of bright and faint components.

four corrected values of log ρ, given in the last line of Table VIII, represent the best mean values of atmospheric density to be derived from the present material. They apply at the corresponding mean heights in the table for an average ground temperature of 50°F (301°K). The two lower points lie practically on the adopted density curve so that no change in this curve is suggested below a height of 76 km. The three upper points lie close to a straight line with a slope corresponding to a constant atmospheric temperature of about 250°K. The adopted density curve attains this slope at a height of 78.0 km.

Thus solution II, the final observed curve of log ρ against height, is taken as the adopted curve to a height of 78.0 km and as a straight line corresponding to a constant temperature of 250°K above 78.0 km (see Fig. 3). The upper portion of the $H-\log \rho$ curve has little weight above a height of 100 km. It is expressed by the equation

$$\log \rho = -2.45 - 0.0592H \text{ (km)}. \qquad (32)$$

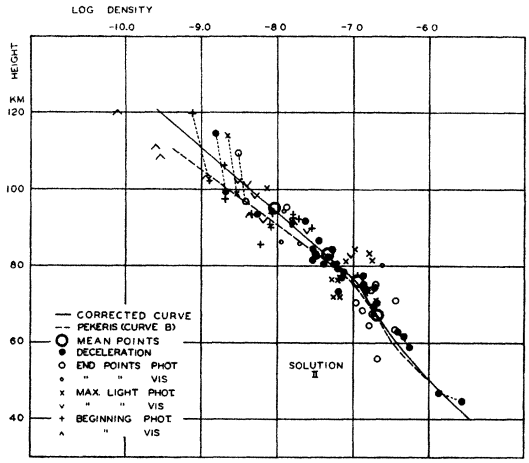

FIG. 3. Density data corrected.

The logarithmic gradient b in natural logarithms per cm is -1.36×10^{-6}.

The interpretation of such a density curve in terms of an atmospheric temperature curve is not mathematically unique. In the practical problem, however (where the height-temperature curve and possibly its slope should be continuous), the range in solution is quite limited. The atmospheric temperature corresponding to the curve of Fig. 3 rises to a flat maximum of 375°K near 62 km and then falls rapidly above 68 km to the 250°K value near 78 km. Without some modification the adopted temperature curve of Fig. 1 cannot be used to a height of 78 km in the interpretation of Fig. 3, because a discontinuity in T would then be required at that height. (Nor should the rate of fall of temperature with height exceed the adiabatic limit of about 10°K per km. The adopted curve in Fig. 1 errs somewhat in this respect.)

The residuals for solution II are given in Table IX; the residuals, in units of 0.01, are contained in columns 3, 6, 9, and 12, respectively, for the density determinations by measures of deceleration, maximum light, first break, and the end point. The determinations by the three latter methods (Table VII) were corrected by Eqs. (31) before the densities of solution II (Table I and Eq. 32) were subtracted from them. It is gratifying to note that the mean residuals for the visual meteors, not used in solution II, are completely satisfied at the end points and maximum light. The mean residual of -0.44 at the beginning points is not disturbing because the meteors may well have been first observed at a later point than was assumed. A possible correction of minus one magnitude in the assumed brightness at first sight or of $+7.5$ km in height will remove the mean residual. Were such corrections required at maximum light or at the end point, the discrepancy would be much more serious.

In order to investigate the correlation of atmospheric densities with ground temperatures, the above-mentioned residuals of Table IX are plotted against $b\Delta T$ (°F$\times10^6$ or °K$\times1.8\times10^6$) in Fig. 4. Only the more reliable data for the photographic meteors are used. A linear correlation would indicate that the region of the upper atmosphere under consideration rises or falls as a whole proportionately to the ground temperature, averaged, as mentioned above, over 48 hours. From a casual inspection of Fig. 4 it can be seen that the deceleration residuals, which are the most reliable, indicate a strong positive correlation while the other residuals suggest none. The beginning points, indeed, exhibit a negative correlation. The solution, consequently, depends strongly upon the weights ascribed to the various sets of density determinations. When the more precise deceleration determinations (V_0' greater than four times its probable error) are given weight four as compared to unity for all other photographic determinations, an increase of 1°K in the mean ground temperature is found to produce a rise of $+0.19\pm0.04$ km. This solution is indicated by the straight line in Fig. 4. The resulting total range of the average seasonal variation in the height of the upper atmosphere is then 5.3 ± 1.0 km. From visual observations of meteors, Öpik obtained 3.7 ± 0.7 km for the corresponding quantity in the region of Flagstaff, Arizona.[28]

Table IX contains the finally-corrected determinations of density in columns 4, 7, 10, and

TABLE VIII. Data for each of the four groups.

Group	I	II	III	IV
H limits km	58–72.0	72.1–80.0	80.1–90.0	>90.0
Mean H km	67.1	75.9	83.1	94.9
Mean $\Delta \log \rho$	0.00	+0.03	+0.12	+0.38
Corrected $\log \rho$	−6.68	−6.95	−7.34	−8.05

[28] E. Öpik, Harvard Ann. **105**, 585 (1937).

TABLE IX. Solution II. Densities and residuals.

Meteor number	Temp. °F	Deceleration			Max. light			First break			End point		
		$\Delta_1 \log \rho_0$	$-\log \rho_0$ corr.	$\Delta_2 \log \rho_0$	$\Delta_1 \log \rho_m$	$-\log \rho_m$ corr.	$\Delta_2 \log \rho_m$	$\Delta_1 \log \rho_1$	$-\log \rho_1$ corr.	$\Delta_2 \log \rho_1$	$\Delta_1 \log \rho_e$	$-\log \rho_e$ corr.	$\Delta_2 \log \rho_e$
Photographic Meteors													
642	+14	+9	7.33	0	−5	7.18	−14	−22	8.09	−31	+25	6.77	+16
642		+28	6.87	+19									
651	−18	−21	7.53	+9	+34	6.98	+46	+6	7.80	+18	+17	6.71	+25
660	−28	0	6.26	+12									
660		+2	6.41	+13									
663	−21	(+29)	(8.82)	(+42)	(+41)	(8.66)	(+54)	(+28)	(9.13)	(+41)	(+28)	(8.52)	(+41)
663		(−47)	(8.68)	(−34)	(−35)	(8.53)	(−22)	(−54)	(8.90)	(−41)	(−38)	(8.43)	(−25)
670	−21	+11	6.72	+19	(−3)	6.71	(+4)	0	6.94	+12	+31	6.44	+38
689	+22	+38	7.64	+24	+20	7.81	+6	−33	8.69	−47	+2	7.51	−12
694	−2				+24	8.14	+25	+3	8.70	+4	+20	7.88	+21
697	+4	−2	7.26	−4	−20	7.22	−22	−25	8.10	−27	−7	6.88	−8
697		+9	6.87	+6									
705	−7	+7	7.46	+12	(+53)	(6.80)	(+58)	(−43)	8.36	(−38)	(−31)	(6.68)	(−28)
705		−8	7.13	−3									
705		+3	6.72	+5									
705		+13	6.33	+16									
710	−1	−17	7.39	−17	−43	7.27	−43	+18	7.73	+18	+2	6.75	+2
710		+7	6.85	+7									
712	+3	−4	7.21	−6	+3	6.85	+2	−4	8.07	−6	+11	6.46	+10
712		+12	6.69	+10									
716	+3				+53	6.76	+51						
727	−25	−30	7.49	−14	−40	7.29	−28	+5	7.56	+21	−1	6.86	+10
730	−27	−42	7.20	−32									
733	−27	−45	8.27	−28									
736	−29	−45	7.54	−27	−3	7.11	+15	−3	7.79	+15	−26	6.97	−17
778	+1	−12	7.16	−12	−34	7.18	−34	−71	8.23	−71	−12	6.79	−12
505*	−11	(−4)	5.83										
505*		(+16)	5.72										
P.E.		±16		±11	±21		±20	±19		±21	±12		±12
Visual Meteors													
Leo.	0				+5			−58			+11		
Per.	0				−3			−61			+1		
a	0				−1			−69			−40		
b	0				−29			−40			−17		
c	0				+10			−42			+1		
d	0				+31			+4			+58		
Mean					+2			−44			+2		

13. The determinations of Table VII have been corrected for the systematic effects of Eqs. (31) and the ground-temperature effect of the preceding paragraph. Values in parenthesis in Table IX have not been used in the numerical solutions, but are portrayed graphically, along with the more precise data, in Fig. 3. Final residuals from solution II are given in columns 5, 8, 11, and 14 of Table IX. The probable errors in $\log \rho$ are satisfactorily small, ±0.11 for single determinations from decelerations, ±0.12 from end points, ±0.20 from maximum light, and ±0.21 from first-break measures. The relative weights are more or less as anticipated.

Of some interest is a third solution, the details of which need not be included in tabular or graphical form. The deceleration values of $\log \rho_0$ were used alone and a least-squares solution made simultaneously for a linear $H - \log \rho$ relation and the ground-temperature effect. The derived temperature of the upper atmosphere was 256°K and the total seasonal amplitude 10 km. The probable error of a single value of $\log \rho$ for the deceleration determinations was only ±0.08, somewhat

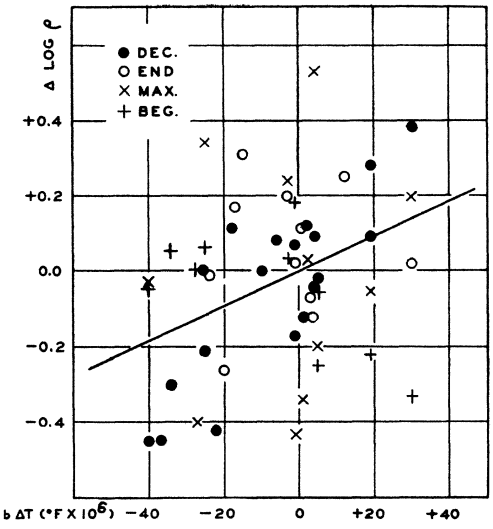

FIG. 4. Seasonal effect.

smaller than from solution II, but the other probable errors were appreciably greater, ±0.19 for end point, ±0.20 for maximum light, and ±0.27 for first-break measures.

We may conclude, therefore, that the present measures of density yield an upper-atmosphere temperature of approximately 250°K in the regions from about 80 km to 95 km. The data favor the existence of a high temperature zone near or slightly above the 60-km level, but are not conclusive in this respect. The average temperature of 256°K from 60 km to 95 km, discussed in the preceding paragraph, may be considered as a minimum value within the likely range of solution. The observations offer no sensitive criterion as to the existence of a narrow region of low temperature near the 82-km level.

Correlations of residuals with functions of the lunar hour angle show no evidence of lunar tides in the upper atmosphere.

5. METEORIC LIGHT CURVES

Some additional information concerning atmospheric densities is provided by studies of single meteor trails in the Harvard collection. Miss Hoffleit[29] discovered that for shower meteors the point of maximum light moves progressively forward along the trail with increase of velocity. Random deviations, representing idiosyncrasies of individual meteors, are large but the effect is well established statistically. A recent study from more extensive material has been made by J. F. Foster[30] who has included a correction for projection effects in each meteor trail. Table X contains his results; column three presents the fraction of the distance along the trail at which maximum light occurs for the meteor showers listed in column one; mean velocities are given in column two while the numbers of trails measured are given in the fourth column. The progressive increase of the position of maximum light with increasing velocity is apparent.

For an atmosphere possessing a constant logarithmic density gradient with height, i.e., a constant temperature, the preceding theory provides theoretical light curves in which the relative position of maximum light is almost independent of the meteoric velocity. If, for the moment, we neglect the meteoric deceleration, which introduces only a minor secondary effect, the light curve of a meteor may be expressed in the general form [from Eqs. (10), (12), (17), (18)]:

$$\frac{\text{Light}}{\text{Light Max.}}=\frac{9}{4}\left(1-\frac{\rho}{3\rho_m}\right)^2\frac{\rho}{\rho_m}. \qquad (33)$$

Thus, with the neglect of meteoric deceleration in an atmosphere of constant temperature, the relative position of maximum light is independent of atmospheric temperature, meteoric velocity, meteoric mass, and direction of fall. Equation (33) leads to a light curve of the general form shown approximately by the two uppermost light curves in Fig. 5 ($V=60$ and 72 km/sec.). The relative position of maximum light depends upon the magnitude range covered in a given trail. For magnitude ranges of one, two, and three magnitudes, the positions of maximum light are 0.68, 0.74, and 0.78, respectively. Foster observed a

TABLE X. Position of maximum light in meteor trails.

Shower	Observational			Theoretical		
	V km sec.$^{-1}$	Max. light	No. trails	1^m range Max. L.	2^m range Max. L.	3^m range Max L.
Taurid	30	0.66	25	0.55	0.60	0.63
Geminid	36	0.60	39	0.62	0.68	0.72
α Aquariid	50	0.64	8	—	—	—
Perseid	61	0.72	25	0.73	0.78	0.81
Orionid	68	0.74	19	—	—	—
Leonid	72	0.81	29	0.69	0.76	0.79

[29] D. Hoffleit, Proc. Nat. Acad. Sci. **19**, 212 (1933).

[30] J. F. Foster, Harvard Bull. No. 916 (1942).

similar relation for actual meteor trails although he did not determine numerical values for the dependence upon magnitude range. There can be no doubt observationally concerning this general characteristic of photographic meteor trails; the decline in brightness is much more abrupt than the rise although individual trails show pronounced deviations from the average.

The effect of deceleration, neglected in Eq. (33), is theoretically negligible throughout most of a meteor trail until near the end. Deceleration extends the trail to slightly lower heights and is more effective for slow than for fast meteors of a given magnitude and magnitude range. Deceleration acts theoretically in the direction of the effect observed by Miss Hoffleit and Foster, but is numerically insufficient to explain the effect. No variation in the fundamental constants, moreover, can be made in order that deceleration may become more operative in determining the position of maximum light. This significant fact deserves more careful consideration.

A close study of the pertinent equations (10), (8), and (12) will show that deceleration affects the relative position of maximum light only via the constant term $\lambda/\gamma\zeta$ in Eq. (8). In an isothermal atmosphere variations in the other constants will affect meteoric heights or intensities systematically, without changing the relative position of maximum light. Hence $\lambda/\gamma\zeta$ must be changed appreciably to account for Miss Hoffleit's result. But a comparison of the equations used in determining the atmospheric densities by means of the four methods, Eqs. (15), (21), (24), and (29), shows that only $\lambda/\gamma\zeta$ can be determined by intercomparing the resultant values of atmospheric density. The ratios of ρ_0 to ρ_m, ρ_1, and ρ_e involve the significant term $(\lambda/\gamma\zeta)^{\frac{1}{2}}$ in all three cases. From the numerical equations (31) we see that no appreciable correction to $\lambda/\gamma\zeta$ is suggested, and, therefore, that in an isothermal atmosphere only a fundamental change in the theory can permit an explanation of the systematic variation with velocity of the position of maximum light.

Suitable temperature gradients in the atmosphere, however, can account for the observations. A meteoroid entering a region where the atmospheric temperature is increasing with height will encounter a continuously increasing logarithmic density gradient and so will have its point of maximum light displaced towards the end of its trail; and conversely in a region where the atmospheric temperature decreases with height. Figure 5 depicts theoretical light curves for meteors of various velocities in the adopted atmosphere (Table I). Masses were chosen to give roughly a constant photographic effect at maximum light. The differences in shape among the various light curves in Fig. 5 are produced almost entirely by the assumed temperature gradients in the atmosphere; the effect of deceleration has been rigorously taken into account by a simple form of numerical integration. In the curve at $V=20$ km/sec. the shape of the flat maximum is highly dependent upon the value of the mass. More massive meteoroids would pass through the high temperature zone and show a maximum quite near the ends of their trails. Less massive meteoroids would show a maximum near the beginning of the flat portion of the curve shown in Fig. 5. This effect is closely related to the argument first presented by Lindemann and Dobson for visual meteors. They found that the end points of visual meteors tended to avoid the 60-km level. Öpik's analysis of the visual meteor observations made by the Arizona expedition for the study of meteors, however, failed to confirm the result obtained by Lindemann and Dobson.

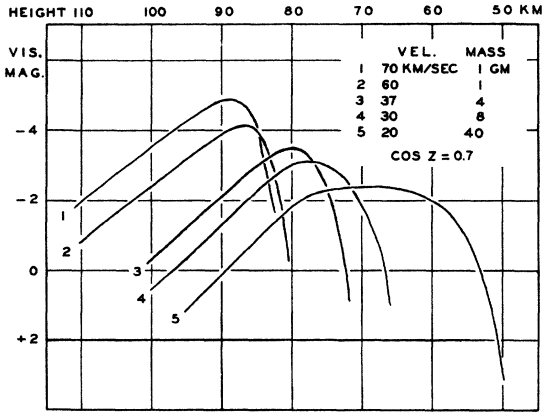

FIG. 5. Theoretical meteor light curves.

The positions of maximum light in the curves of Fig. 5 are given in the last three columns of Table X for three values of the range in bright-

ness. Probably a two-magnitude range most closely approximates that for an average meteor trail studied by Foster. The agreement with his observed increase in the position of maximum light with increasing velocity is fairly satisfactory, except for the theoretical inversion from velocity 60 to 72 km/sec. This inversion arises from the low temperature zone at 82 km assumed in the adopted atmosphere. Foster's observed inversion between the Taurid and Geminid showers would be very difficult to explain by temperature gradients in the atmosphere. It may be explained by physical differences between the meteoroids in the two showers or as a random error of observation.

The observations of the position of maximum light in photographic meteor trails, therefore, require a high temperature zone near the 60-km level in the atmosphere, but are better satisfied without the low temperature zone at the 82-km level. The derived atmospheric density curve of Fig. 3 or Pekeris' density curve 13 of Fig. 2 are, consequently, more satisfactory than the adopted density curve of Table I and Fig. 2.

6. SUMMARY

Section 1 outlines briefly the evidence concerning the construction and temperature of the upper atmosphere from a height of 40 to 110 km. A high temperature zone (270°±K) near 60 km, a minimum (160°K) near 82 km, and a continual rise in temperature above this level have been indicated by other researches. These temperatures and the discussion in the present paper are based on the assumption of a constant mean molecular weight throughout the relevant layers of the atmosphere.

The observational material for photographic and visual meteors is described and presented in Sections 1 and 2. Meteoric velocities have been determined for some 17 photographic meteors by the two-camera rotating-shutter method. Decelerations have been measured near the central point of most of these trails and in some cases at more than one point. Heights, magnitudes, and other pertinent data are given at various significant points along the trails. Somewhat similar data for visual meteors have been included from Öpik's studies of the data from the Arizona expedition for the study of meteors.

The adopted theory used in the determinations of atmospheric densities from meteor data, photographic and visual, is presented in Section 3. Formulae are derived for density calculations at four points along a trail, near the beginning, at maximum light, at the end, and at any point where the deceleration is measurable. The assumptions and physical constants of the theory are discussed in some detail.

The resultant determinations of atmospheric density (ρ) are contained in Section 4. Comparisons of the densities derived by the four methods for each trail indicate that the systematic deviations between the methods are generally less than 0.1 in $\log \rho$. Single determinations of $\log \rho$ show probable errors of the order of ± 0.12 for deceleration and end-point values and ± 0.21 for the beginning and maximum light values. The results from visual observations are consistent with the photographic results. The solution for the height $-\log \rho$ curve is coupled with the solution for a seasonal or ground-temperature effect. A considerable range of solution occurs, depending upon the weighting ascribed to the various methods of determining the atmospheric density. The best solution appears to be one in which the height $-\log \rho$ curve corresponds to a flat temperature maximum of about 375°K near the 60-km level, a rapid drop to 250°K near 80 km, and a constant or slowly rising temperature at greater heights to about 110 km. The corresponding seasonal effect indicates that the upper atmosphere is raised 5.3 ± 1.0 km under average midsummer temperatures as compared to its height under average midwinter temperatures.

It must be noted, however, that a constant atmospheric temperature of about 256°K from 60 km to 110 km is not entirely outside the range of solution. The corresponding seasonal effect is considerably greater than that given above.

On the other hand, observations by Miss Hoffleit and Foster of the relative position of the point of maximum light in singly photographed meteor trails cannot be explained by the present theory in terms of a constant temperature in the upper atmosphere. The discussion in Section 5 shows that a high temperature zone near the 60-km level is required to account for these observations and that a conspicuous temperature minimum near 82 km is not indicated.